Journal of Power Sources 190 (2009) 230–240

Contents lists available at ScienceDirect

Journal of Power Sources

journal homepage: www.elsevier.com/locate/jpowsour

Experimental study on water transport coefficient in Proton Exchange Membrane Fuel Cell

T. Colinart[a], A. Chenu[a], S. Didierjean[a,*], O. Lottin[a], S. Besse[b]

[a] LEMTA – UMR 7563 CNRS Nancy-University, 2, avenue de la Forêt de Haye, BP 160, 54504 Vandoeuvre-lès-Nancy cedex, France
[b] HELION Hydrogen Power, Domaine du Petit Arbois, Bâtiment Jules Verne, BP71, 13545 Aix en Provence, France

ARTICLE INFO

Article history:
Received 14 November 2008
Received in revised form 27 December 2008
Accepted 18 January 2009
Available online 23 February 2009

Keywords:
PEM fuel cells
Water transport coefficient
Water management
Experimental study

ABSTRACT

Water transport within Proton Exchange Membrane Fuel Cell (PEMFC) is investigated by systematic measurements of the water transport coefficient, defined as the net water flux across the membrane divided by the water production. It is recorded for various operating conditions (current density, gas stoichiometry, air inlet relative humidity, temperature, pressure) in a fuel cell stack fed by dry hydrogen. The measurement of the water transport coefficient shows that a significant fraction of water is collected at the anode while water is produced or injected at the cathode. Moreover, in usual operating conditions, liquid water is present at the cell outlet not only in the cathode but also in the anode. Contrary to the electrical performances, ageing has no influence on the water transport coefficient, which allows the comparison between data collected at different periods of the fuel cell lifetime. From this comparison, it was found that the hydrogen flow rate, the amount of vapor injected at cathode inlet, and the temperature are the main parameters influencing the water transport coefficient. It is shown that air and hydrogen stoichiometry present significant effects on water transport but only through these parameters.

1. Introduction

Despite of recent advances in PEM fuel cell technology their large-scale commercialization is still hampered by the cost of materials (such as ionomer membranes and platinum-based electrodes) and by their low reliability (in terms of early failure modes and relatively short durability) [1,2].

In this context, water management has become one of the crucial aspects in the design and operation of PEMFCs. The challenge of water management was addressed in many ways: membrane–electrode assembly designs, flow-field designs or new humidification strategies [3]. The optimal stationary operation of a PEM fuel cell results from a compromise between two effects:

- The ionic conductivity of the proton-conducting membranes is strongly dependent on their water content. When membrane dehydration or drying occurs, the electrical performances drop due to significant ohmic losses [4].
- However, an excess of water is also to be avoided due to condensation. Liquid water hinders the transport of oxygen by blocking the pores of the gas diffusion layers (GDL), covers up active sites in the catalyst layers and plugs the gas transport channels in the flow-field plates. Water flooding results in a non-uniform distribution of reactants over the active catalyst area and leads to poor electrical performances [5,6].

Therefore, it is essential to identify the mechanisms contributing to the water transport within the different elements of a cell. As shown in Fig. 1, water transport occurs within various components of diverse shape and structure. It is generally accepted that there is at least three mechanisms at stake:

- Diffusion of water vapor from the most to the less humid regions.
- Electro-osmotic drag, from the anode to the cathode.
- Hydraulic permeation due to pressure gradient.

In two-phase conditions, additional modes of water transport appear:

- Capillary flow of liquid water within the GDL.
- Water droplets formation and detachment at the GDL-gas channel interface.
- Liquid film flow on the channel walls.

There are various ways of studying water transport within fuel cell:

* Corresponding author. Tel.: +33 3 83 59 55 60; fax: +33 3 83 59 55 51.
E-mail address: Sophie.didierjean@ensem.inpl-nancy.fr (S. Didierjean).

0378-7753/$ – see front matter © 2009 Elsevier B.V. All rights reserved.
doi:10.1016/j.jpowsour.2009.01.038

Nomenclature

$D^m_{H_2O}$	water diffusion coefficient in the membrane ($m^2\ s^{-1}$)
E_m	membrane thickness (m)
EW	membrane equivalent weight ($g\ mol^{-1}$)
F	Faraday constant (C)
j	current density ($A\ cm^{-2}$)
$N^a_{H_2O}$	water collected at the anode ($mol\ cm^{-2}\ s^{-1}$)
$N^{a\ vap}_{H_2O}$	saturated vapor removed by the anode exhaust ($mol\ cm^{-2}\ s^{-1}$)
$N^c_{H_2O}$	water collected at the cathode ($mol\ cm^{-2}\ s^{-1}$)
$N^{c\ vap}_{H_2O}$	saturated vapor removed by the cathode exhaust ($mol\ cm^{-2}\ s^{-1}$)
$N^{Hum}_{H_2O}$	air inlet humidification flow rate ($mol\ cm^{-2}\ s^{-1}$)
$N^{prod}_{H_2O}$	produced water ($mol\ cm^{-2}\ s^{-1}$)
$N^{Diff}_{H_2O}$	diffusive water flux in the membrane ($mol\ cm^{-2}\ s^{-1}$)
N^{in}_{Air}	air inlet flow rate ($mol\ cm^{-2}\ s^{-1}$)
$N^{in}_{H_2}$	hydrogen inlet flow rate ($mol\ cm^{-2}\ s^{-1}$)
$p_{sat}(T)$	saturation pressure (bar)
P	pressure (bar)
RH_c	air relative humidity (−)
T	temperature (°C)
$x^{in}_{O_2}$	inlet molar fraction of oxygen (−)

Greek letters

α	water transport coefficient (−)
λ	membrane water content (−)
λ_{Air}	stoichiometric ratio of air (−)
λ_{H_2}	stoichiometric ratio of hydrogen (−)
ρ_{dry}	membrane density ($g\ m^{-3}$)

- theoretical investigation and modelling [8–14],
- in-situ determination of the local water concentration [15–20],
- and experimental determination of a global water transport coefficient, as a function of the amount of water introduced into the fuel cell, produced by the electrochemical reaction, and recovered at the exit of the electrode channels.

In the last case, the authors consider generally two coefficients:

- A water transport coefficient α, defined as the net water flux across the membrane divided by the water production.
- An effective electro-osmotic drag coefficient or net drag coefficient n_d, defined as the net number of water molecules transported per proton.

Theses two coefficients are related by a factor −2 so that: $\alpha = -2n_d$.

The objective of this paper is to explore experimentally the significance of the operating parameters on water transport. In this regard, the results provide new insight into water management in PEMFC.

A literature review related to water management and to the water transport coefficient is presented in Section 2. The Section 3 contains definitions and presents the measurement methodology. In Section 4, results are presented and discussed. They are obtained using different humidification strategies involving the gas stoichiometric ratios, the cathode inlet humidification flow rate or the fuel cell temperature. Section 5 summarizes the results and concludes the paper.

2. Literature review on water transport coefficient

Experimental studies on water transport in PEM fuel cells were reported by several groups [21–44]. Most often, water exiting the fuel cell is condensed, collected and weighed. The Table 1 presents a synthesis of the experimental results, expressed in term of water transport coefficient α. The experimental conditions (including the operating conditions and the type of fuel cell or their components) are very heterogeneous and make the comparison between these studies difficult. However, some common trends appear: they are discussed below.

2.1. Effects of material and components

The choice of fuel cell components affects water transport. Janssen and Overvelde [25] measured the effective electro-osmotic drag coefficient with various MEAs made with Nafion 112 and Nafion 105 and three types of electrodes: E-Tek DS, E-Tek SS and Toray. They show that whatever the operating conditions, the

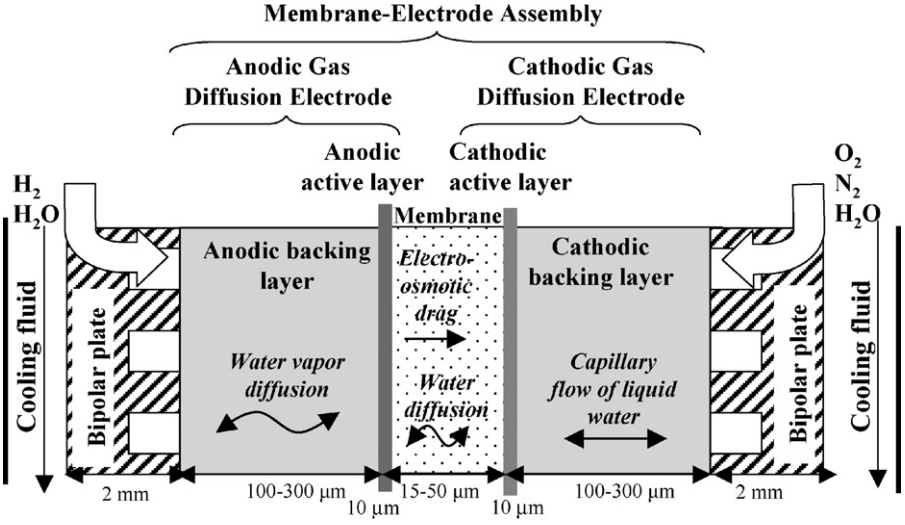

Fig. 1. Water transport mechanisms in fuel cell MEA [7].

Table 1
Literature review of the water transport coefficient α, defined as the net water flux across the membrane divided by the water production. The arrows indicate the evolution of α with an increase of each parametric value.

Authors	Material	T (°C)	P_a - P_c (bar)	λ_{H_2}	RH_{H_2}	λ_{Air}	RH_{Air}	i (A.cm^{-2})	Remarks
[27] Mennola et al.	GORE Primea 25 cm²	40 - 60		1.5 - 2.5 α ↗	0	1	0.1 ... 0.2	0.1 - 0.2 α ↗	Free-breathing PEMFC
[34] Lu et al.	GORE 30 μm 6 cm² co-flow	80	2	2	1	2	0.3	1	Study on spatially resolved water crossover coefficient
[35] Liu et al.	GORE 30 μm 6 cm² co-flow	80	2	2	0 - 0.42 α ↘	2	0 - 0.42 α ↗	1	Study on spatially resolved water crossover coefficient
[30] Murahashi et al.	Nafion 112 25 cm² counter-flow	70 - 80 α ↗		1.43	0.42	2	0.42 - 0.8 α ↗	0.3	
[32] Atiyeh et al.	Nafion 112 100 cm²	60	1.35	1.4	0.6 - 1	2 - 3	1 - 0.6	0.3 - 0.7 α ↘	Investigation of the role of a microporous layer
[33] Karan et al.	Nafion 112 100 cm²	60	1.35	1.4	0.6 - 1	2 - 3	1 - 0.6	0.3 - 0.7 α ↘	Investigation of the role of a microporous layer at the cathode
[25] Janssen and Overvelde	Nafion 105 - 112 50 cm² counter-flow	60	1.5 - 3	1.5 - 4 α ↗	0	2	1	0.4 - 0.6 α ↗	Wide range of operating conditions Different types of MEA
[28] Cai et al.	Nafion 112 - 115 128 cm² Co-flow	60	2	1.1	0 - 0.75 α ↗	2.5	0.56	0.1 - 0.6 α ↗	Tanaka electrodes Liquid water at the cell outlet
[22] Büchi and Srinivasan	Nafion 115 50 cm² counter-flow	40 - 75 α ↗	1 - 1.7	1.7 - 4.4 α ↗	0	1.2 - 4.5 α →	0	0.1 - 0.3 α ↘	E-tek electrodes Hydrogen saturated at the cell outlet
[26] Ciureanu and Badita	Nafion 105 250 cm² 5-cells stack	52	1	?	0	4	0.4	0.04 - 0.4 α ↗	Wide range of operating conditions Liquid water at the cell outlet
[29] Yan et al.	Nafion 117 25 cm²	80	1	1 - 3 α ↗	0.1 - 1 α ↗	2	0.1 - 1 α ↘	0.1 - 0.7 α ↗	E-tek electrodes
[31] Jeong et al.	Nafion 221 25 cm²	25 - 35 α ↘		2.5 - 5 α ↗	0	1	0.3 - 1 α ↗	0.05 - 0.2 α ↗	Free-breathing PEMFC

Thickness of the membrane: Nafion 112: 50 μm; Nafion 105 or 115: 125 μm; Nafion 117: 170 μm.

amount of water collected at the anode side increases when the membrane is the thinnest (50 μm *vs.* 125 μm), which reflects a better diffusion through the membrane. On the other hand, the use of different electrodes has only a minor effect on the water transport, which was attributed to their hydrophobic character and to the presence of an additional microporous layer (MPL). Atiyeh et al. [32] and Karan et al. [33] studied the role of the MPL in water transport at various operating conditions. The MPLs were used at either one or both electrodes. They show that the addition of a MPL at the cathode does not modify significantly the effective electro-osmotic drag coefficient, but that it is at the origin of an important improvement of the fuel cell performance and durability. However, the presence of a MPL at the anode alone or at both electrodes improves water removal through the hydrogen channels and lowers the effective electro-osmotic drag coefficient.

2.2. Effects of the operating conditions

Despite of a variety of operating conditions, the results from experimental studies on water transport in PEMFCs (Table 1) show some common trends in the effects associated with the main operating parameters. Values are mentioned only for fuel cells operated with dry hydrogen.

- An increase in the hydrogen stoichiometry reduces the net drag coefficient, which can even reach negative values: the effective electro-osmotic drag coefficient measured by Janssen and Overvelde [25] drops from −0.2 to −0.3 when the hydrogen stoichiometry increases from 1.5 to 4. Similar results were observed by Ciureanu and Badita [26] on a 5-cells stack.
- The effect of the air stoichiometry is not so clear: in [22], the water transport coefficient seems independent on dry air stoichiometry in the range 1.2–4.5. If the air is humidified, according to Atiyeh et al. [32], the amount of water removed at the anode side decreases with higher air flow rates. They attributed this result to the enhancement of water removal by the airflow.
- An increase in the air hygrometry leads to a decrease of n_d [29–31], which can take positive or negative values depending on the hydrogen relative humidity. On the contrary, an increase in the hydrogen hygrometry improves the net drag coefficient [28,34,35].

- Likewise, the anode water removal significantly increases with the cell temperature [22,27,31]. With dry gases, Büchi and Srinivasan [22] found that the water transport coefficient decreases from −0.04 at 40 °C to −0.3 at 75 °C.
- The majority of the authors do not consider the effect of pressure. Yan et al. [29] observed a small reduction in the net drag coefficient when they applied higher pressure at the cathode than at the anode. Water transport through hydraulic permeation is very limited compared to electro-osmotic drag and back diffusion.
- If dry hydrogen is used, the water transport coefficient increases with the current density [26,28,31], or shows only slight variations if air is also dry [22].

Cai et al. [28] measured the net water drag coefficient in a fuel cell fed by dry hydrogen and wet air (HR = 56%) with H_2/air stoichiometric ratio of 1.1/2.5. The operating temperature and pressure were 60 °C and 2 bar. The MEA had an active area of 128 cm^2 and consisted of Nafion 112 and homemade electrodes with a MPL. They found that the amount of water collected at the anode rises from 12% to 37% with a current density increasing from 0.1 to 0.6 A cm^{-2}.

Mennola et al. [27] studied water balance with a free-breathing PEMFC oriented in the vertical direction and they focused on the anode parameters. Measurements were performed using two different directions of hydrogen flow: hydrogen entering at an upper corner and exiting at the opposite lower corner and vice-versa. When hydrogen enters from a lower corner, the amount of water collected at the anode side is lower and the electrical performances are better than in the other case: the authors assumed that there is an internal water redistribution which maintains the membrane fully humidified. To our knowledge, no comparison between co-flow and counter-flow configurations has been published yet.

2.3. State of water at fuel cell outlets

In most of the cases, no information is provided about the state of water at the cell outlet. However, Ciureanu and Badita [26] and Cai et al. [28] mentioned that liquid water is present at the cell outlet, except at very low current density ($j < 0.04$ A cm^{-2}), even under low air humidification [28]. Cai et al. [28] also indicated that when the air relative humidity increases from 30% to 100%, the fraction of liquid water at the cathode outlet (respectively at the anode outlet) changes from 35% to 55% (respectively from 77.5% to 85%). This trend was confirmed by Bonnet et al. [21], who conducted experiments with a single cell and with a 5-cells stack and investigated the effects of the stoichiometric ratio: the amount of liquid water at both electrodes decreases when the air or hydrogen stoichiometric ratio increases; when the air stoichiometric ratio reaches 3.5, no more liquid water is observed at the cathode outlet. They observed that the fraction of liquid is generally higher at the anode than at the cathode.

2.4. Conclusion of the literature review

This literature review shows that there are only a small number of published experimental studies on water management and water transport coefficient in PEMFC. Due to the variety of experimental conditions and materials, no general strategy for water management in PEMFCs can be deduced from these results. However, water removal through the anode outlet can be enhanced by:

- increasing the hydrogen stoichiometric ratio;
- decreasing the air stoichiometric ratio;
- maintaining a lower relative humidity at the anode than at the cathode;
- increasing the cell temperature or the current density;
- reducing the membrane thickness or including a MPL at the anode side.

It must be emphasized that the influence of other parameters like the gravity – the position of the cell –, the design of the flow-field plates or the mechanical compression is not well understood.

One of the objectives of this work is to analyse reliable experimental data obtained with a single system for investigating the influence of the operating parameters.

3. Methodology

3.1. Experimental set-up

All the experiments presented below were carried out within the framework of the SPACT-80 project, which was already presented in a previous paper [21]. One of the main results of this project is the similarity in behaviour between a 25 cm^2 single cell and a 340 cm^2/5-cells pilot stack (in terms of electrical performances and water management). Their behaviour and performances are also representative of those of a 800 cm^2/90-cells stack. Therefore, this paper details some experimental results obtained with the 340 cm^2/5-cells pilot stack and the analysis concerns only water management. The fuel cell stack was supplied by the manufacturer and project leader Helion [45]. Its architecture was designed in order to match the technical requirements of two testing platforms. A thin perfluorosulfonated membrane and gas diffusion layers coated with microporous layer were selected among several suppliers in order to reach 0.68 V per cell at $j = 0.54$ A cm^{-2}.

The temperature of the fuel cell water-cooling circuit was set to the selected value with a PID controller. A temperature difference lower than 2 °C was observed between the cooling water inlet and outlet. Pure H_2 and air were supplied to the anode and cathode, respectively, in a current-based flow control mode such as the stoichiometric ratio of H_2 and air were fixed. However, because of patent rights, no information can be given about the design of the flow-field plates. The pressure of the reactant gases was maintained between 1 and 1.6 bar. Air was humidified through a Controlled Evaporation and Mixing system (Bronkhorst). The relative humidity of the inlet gases was controlled through the mass flow rate of evaporated water. Lines between humidifiers and the fuel cell were heated in order to avoid water condensation. The gas mass flow rates were regulated at the fuel cell inlets whereas the pressure was controlled at the outlets. The reference operating conditions are summarized in Table 2.

The system is equipped with a water collection system for both anode and cathode effluent streams. The water at the cell outlet is condensed at 5 ± 0.1 °C in a cold trap and the amounts of collected water are continuously weighted. $N^a_{H_2O}$ and $N^c_{H_2O}$ stand for the flow rate of water removed at the anode and at the cathode outlets. An overall water balance was performed, accounting for the amount of water produced by the electrochemical reaction and supplied for the humidification of air, in order to assess the reliability of the experimental results (Fig. 2). More than 95% is recovered, whatever the conditions. The fuel cell was operated in steady state (constant voltage) for at least 2 h before the data were recorded.

Table 2
Reference operating conditions.

Temperature, T	70 °C
Pressure, P	1.6 bar
Hydrogen stoichiometric ratio, λ_{H_2}	1.4
Air stoichiometric ratio, λ_{Air}	2
Humidification	Dry hydrogen Air humidified at 70% RH

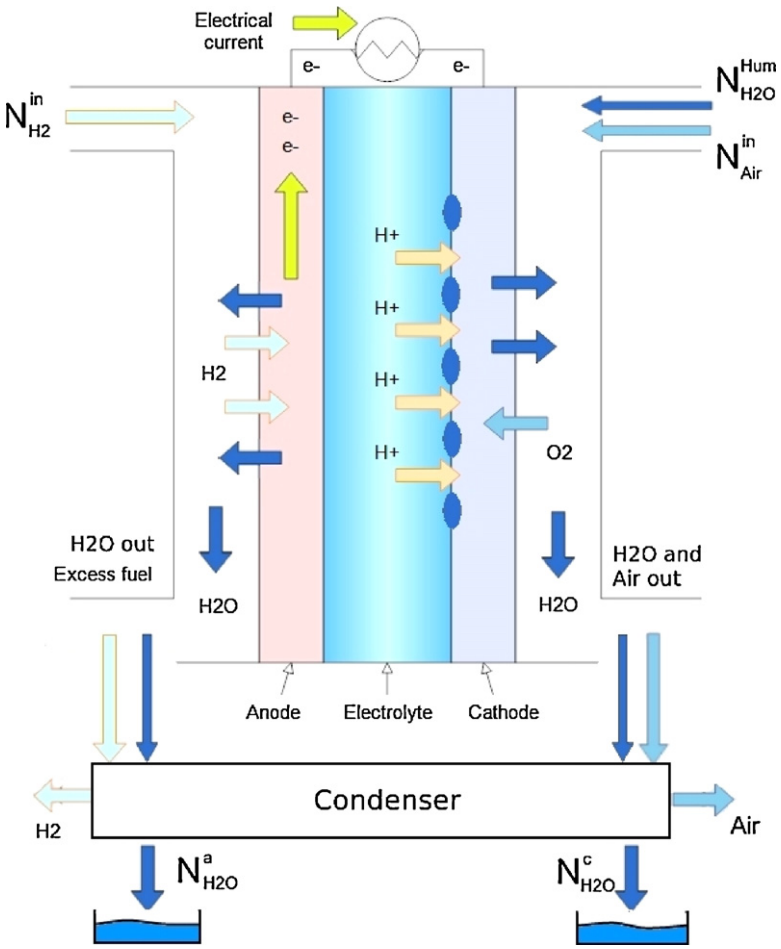

Fig. 2. Schematic representation of the water collection system.

3.2. Water transport coefficient: definition and measurement

The amount of water introduced into the cell with the air is equal to:

$$N^{\text{Hum}}_{H_2O} = N^{\text{in}}_{\text{Air}} \frac{RH_c/100}{(P/p_{\text{sat}}(T)) - (RH_c/100)} \quad (1)$$

with

$$N^{\text{in}}_{\text{Air}} = \frac{\lambda_{\text{Air}}}{x^{\text{in}}_{O_2}} \frac{j}{4F} \quad (2)$$

$N^{\text{Hum}}_{H_2O}$ is proportional to the current density j and to the stoichiometric ratio λ_{Air}. It increases with the temperature T and decreases with the gas pressure P. The water production is also proportional to the current density:

$$N^{\text{prod}}_{H_2O} = \frac{j}{2F} \quad (3)$$

In a stationary state, the amount of water fed and produced is equal to that leaving the cell, i.e. $N^{\text{Hum}}_{H_2O} + N^{\text{prod}}_{H_2O} = N^{a}_{H_2O} + N^{c}_{H_2O}$. Since air is humidified and water is produced at the cathode, collecting water at the anode indicates that a part of it flowed through the membrane. α denotes the water transport coefficient, defined as the ratio between the amount of water transported through the membrane and produced:

$$\alpha = \frac{N^{a}_{H_2O}}{N^{\text{prod}}_{H_2O}} \quad (4)$$

In Fig. 3, α is plotted as a function of the current density for the base-case operation (Table 2). The experimental data are available for current densities higher than $j > 0.2\,\text{A cm}^{-2}$. Below this value, the cell voltage does not stabilize and decreases slightly with time,

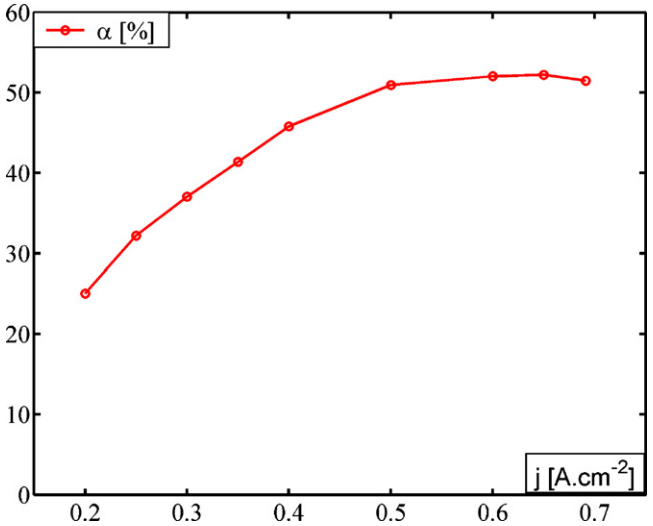

Fig. 3. Variation in α as a function of the current density j for the base-case operation. Fuel cell fed by dry hydrogen and air at 70% RH. $\lambda_{\text{Air}} = 2$; $\lambda_{H_2} = 1.4$, $T = 70\,^{\circ}\text{C}$ and $P = 1.6$ bar.

making it impossible to reach the steady state as well as to collect enough water. Because of technical limitations of the test bench, current densities are not higher than $j > 0.7\ \mathrm{A\,cm^{-2}}$.

Fig. 3 shows that 25–50% of the produced water leaves the fuel cell from the anode outlet in the range of current density of 0.2–0.7 A cm^{-2}. In this same range, Cai et al. [28] measured values of the water transport coefficient varying from 12% to 37%. The differences are due to the operating conditions ($RH_c = 56\%$, $\lambda_{Air} = 2.5$, λ_{H_2} 1.1) and to the materials. However, both profiles are similar in shape, with a steeper slope at low current densities in this work.

Water transport in a fuel cell membrane is dominated by two main mechanisms, namely, electro-osmotic drag caused by the migration of hydrated proton from the anode to the cathode and water diffusion caused by the water concentration gradient between the anode and the cathode. In the present case, since the fuel cell is fed by dry hydrogen, collecting water at the anode side means that the water diffusion is the dominant process.

The water transport coefficient increases with the current density until $j = 0.6\ \mathrm{A\,cm^{-2}}$, which indicates that the back diffusion increases more (with j) than the electro-osmotic drag. Then, it seems to reach a constant value beyond $j = 0.6\ \mathrm{A\,cm^{-2}}$, meaning that the increase of the electro-osmotic drag is offset by the back diffusion. In this work, like in the work of Cai et al. [28], the water drag coefficient begins to decrease, but this result should be corroborated by other experiments conducted at higher current density.

The water flow rates removed at the cell outlet $N^a_{H_2O}$ and $N^c_{H_2O}$ can be directly compared with the amounts of vapor removed from the anode and the cathode $N^{a\ vap}_{H_2O}$ and $N^{c\ vap}_{H_2O}$ in the saturated gases. These amounts are estimated as functions of $p_{sat}(T)$, j and of the stoichiometric ratios λ_{H_2} and λ_{Air} by:

$$N^{a\ vap}_{H_2O} = \frac{1}{P/(p_{sat}(T)) - 1}\left(\lambda_{H_2} - 1\right)\frac{j}{2F} \quad (5)$$

$$N^{c\ vap}_{H_2O} = \frac{1}{P/p_{sat}(T) - 1}\left(\frac{\lambda_{Air}}{x^{in}_{O_2}} - 1\right)\frac{j}{4F} \quad (6)$$

$N^a_{H_2O} > N^{a\ vap}_{H_2O}$ (respectively $N^c_{H_2O} > N^{c\ vap}_{H_2O}$) indicates that a part of water is evacuated in liquid form at the cell outlet.

Fig. 4 shows the fraction of water leaving the cell in liquid form at the anode and the cathode. It can be observed that, in the base-case, liquid water is present at the outlet of both electrodes whatever the current density. 15% to 35% of the water is leaving the cathode in liquid form, whereas this fraction varies between 60% and 80% at the anode. Such high values at the anode can be explained by the low hydrogen flow.

At least several areas of the anode and cathode chambers should be flooded, but the electrical performances do not seem to be affected. Thus, it can be supposed that the outlet part of the anode is flooded and that the diffusion from the cathode is favoured at the inlet part of the cell. This is partially confirmed by Liu et al. [35] who observed that the local water transport coefficient decreases from 25% at the inlet to 12% at the outlet with a fuel cell fed by dry hydrogen and wet air.

In any case, such high amounts of liquid should inhibit at least partially the diffusion of oxygen and hydrogen toward the catalyst layers and it appears necessary to develop experiments allowing localizing water, in parallel with multi-D modelling of the two-phase flows within the cell.

3.3. Aging and water management

The whole of the experiments lasted for 1300 h during which the fuel cell was operated in stationary regime at near nominal conditions. Eventually, the fuel cell had been used for 2000 h.

Fuel cell aging is most often characterized by a reduction in the electrical performances, caused by a degradation of some of its components. Fig. 5a shows four polarization curves recorded at dif-

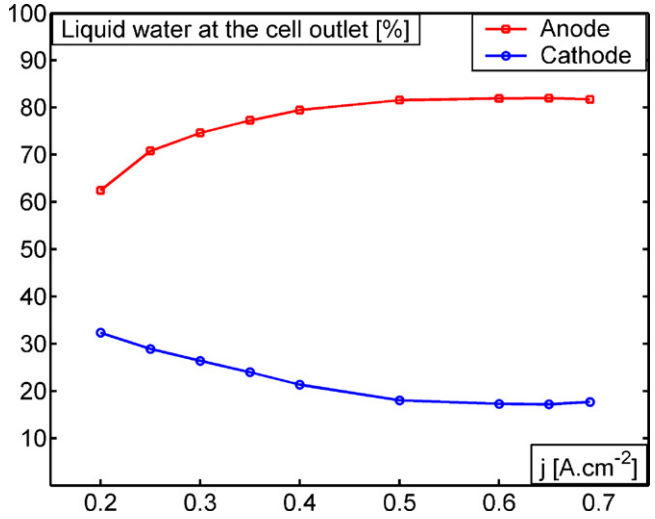

Fig. 4. Liquid to total amounts of water at the cell outlet vs. current density. Fuel cell fed by dry hydrogen and air at 70% RH. $\lambda_{Air} = 2$; $\lambda_{H_2} = 1.4$; $T = 70\ ^\circ$C and $P = 1.6$ bar.

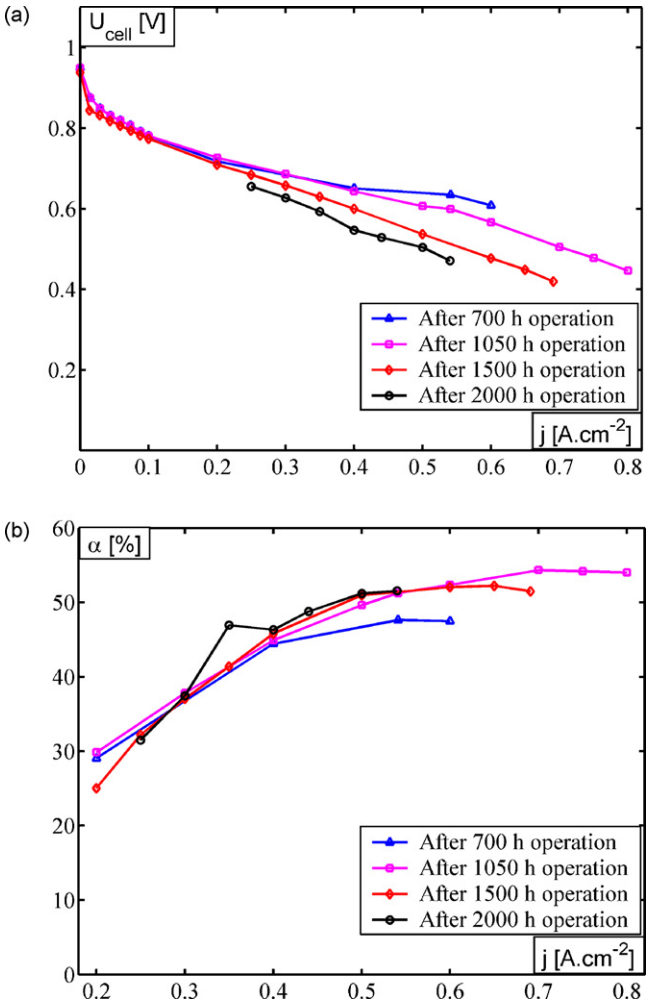

Fig. 5. Polarization curve (a) and water transport coefficient (b)—influence of aging. Fuel cell fed by dry hydrogen and air at 70% RH. $\lambda_{Air} = 2$; $\lambda_{H_2} = 1.4$; $T = 70\ ^\circ$C and $P = 1.6$ bar.

ferent times for the base-case operation. The differences between the four curves are small at low current density but they increase with j. At $j = 0.54\ A\,cm^{-2}$, the degradation rate over 1100 h was about $150\ \mu V\,h^{-1}$, which is higher than the values obtained by the other project partners in steady state operation. Several causes can be mentioned [46]: loss in membrane ionic conductivity, holes in the membrane, migration of catalyst [47,48], loss of catalyst activity, poisoning, deterioration of mass transport properties in the porous layers [49] or corrosion on bipolar plates [50]. The comparison of the cell performances measured in different operating conditions is difficult if the experiments are carried out over several hundredths of hours, which was the case.

However, it is necessary to verify that the comparison between values of the water transport coefficients measured at different times makes sense: Fig. 5b shows four curves corresponding to the base-case operation. Except for few points, the evolutions remain identical. Aging does not affect the global water transport coefficient, which makes the investigation of the influence of each operating parameter possible. As a corollary, the degradation of the MEA is of no consequence in terms of water transfer.

4. Experimental results and discussion

Experiments were performed either at a constant current density (the reference being $j = 0.4\ A\,cm^{-2}$) or by varying the current density. For clarity, the water transport coefficient is plotted as a function of the flow rates of gas or of humidification water at the fuel cell inlet.

4.1. Gas stoichiometric ratio

4.1.1. Hydrogen stoichiometric ratio λ_{H_2}

According to Eq. (7), the hydrogen flow rate $N_{H_2}^{in}$ can be expressed as a function of either the hydrogen stoichiometric ratio λ_{H_2} at constant current density or, λ_{H_2} being kept constant, of the current density only.

$$N_{H_2}^{in} = \lambda_{H_2} \frac{j}{2F} \tag{7}$$

Fig. 6 depicts the evolution of the water transport coefficient vs. the hydrogen flow rate $N_{H_2}^{in}$ in these two conditions: $j = 0.4\ A\,cm^{-2}$ and λ_{H_2} varying continuously from 1.1 to 3 and $\lambda_{H_2} = 1.2$, $\lambda_{H_2} = 1.4$ and $\lambda_{H_2} = 1.6$ while j increases from $j = 0.2\ A\,cm^{-2}$ to $j = 0.7\ A\,cm^{-2}$.

As shown in Fig. 6, the water transport coefficient increases with the hydrogen flow rate at constant current density. This indicates that an increase in $N_{H_2}^{in}$ improves the diffusion of water through the membrane from the cathode side. Büchi and Srinivasan [22] obtained similar results: the water removed from the anode, at a constant air stoichiometry, is found to be a linear function of the hydrogen stoichiometry.

At a constant current density ($j = 0.4\ A\,cm^{-2}$), Bonnet et al. [21] showed that liquid water is present at the outlet of each compartment whatever λ_{H_2}. The fraction of liquid water at the cell outlet decreases from 90% to 40% at the anode and from 28% to 0% at the cathode as the hydrogen stoichiometry increases from 1.1 to 3. An increase in λ_{H_2} or in $N_{H_2}^{in}$ improves water drainage and reduces the amount of liquid water in the anode chamber, which results in a higher diffusion rate from the cathode to the anode and to an increase in α. Since the amount of water produced by the fuel cell remains constant, the ratio of liquid water at the anode outlet decreases also.

Fig. 6 also presents a comparison of the curves obtained by varying the current at constant values of the hydrogen stoichiometric ratio λ_{H_2} (set to 1.2, 1.4 and 1.6). According to Eq. (7), each value of the hydrogen flow rate defines a linear relation between the current density and the hydrogen stoichiometric ratio. For instance, $N_{H_2}^{in} = 2.5\ mol\,cm^{-2}\,s^{-1}$ corresponds to $\lambda_{H_2} = 1.2$ and $j = 0.4\ A\,cm^{-2}$ and to $\lambda_{H_2} = 1.6$ and $j = 0.3\ A\,cm^{-2}$. In Fig. 6, the three curves obtained with $\lambda_{H_2} = 1.2$, $\lambda_{H_2} = 1.4$ and $\lambda_{H_2} = 1.6$ are very close to each other and to the one obtained by varying λ_{H_2} at constant current density. From this result, it can be concluded that in this range of operating conditions, the meaningful parameter that determines the water transfer through the membrane is the hydrogen flow rate $N_{H_2}^{in}$ rather than the current density or the hydrogen stoichiometric ratio.

4.1.2. Air stoichiometric ratio λ_{Air}

The same reasoning applied to the influence of the air stoichiometric ratio λ_{Air} leads to a very different conclusion: it is clear from Fig. 7 that in the range $\lambda_{Air} = 1.5$–4, the water transport coefficient cannot be expressed as a function of the air flow rate only; α is almost independent of the air stoichiometry at constant density ($j = 0.4\ A\,cm^{-2}$) and remains close to 45% while it depends strongly

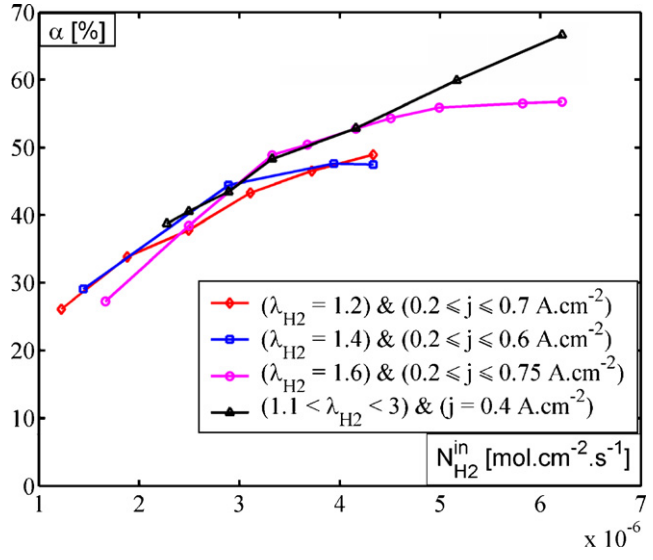

Fig. 6. α as a function of the hydrogen flow rate $N_{H_2}^{in}$ and effect of the hydrogen stoichiometry λ_{H_2}. Fuel cell fed by dry hydrogen and air at 70% RH. $\lambda_{Air} = 2$; $T = 70\ ^\circ C$ and $P = 1.6$ bar.

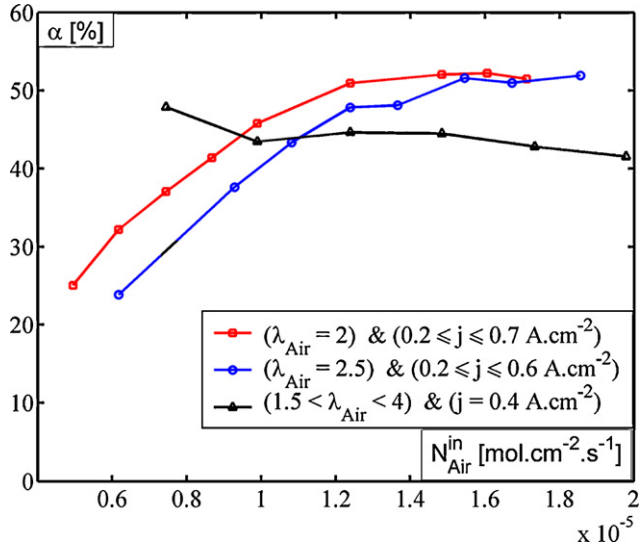

Fig. 7. α vs. the air flow rate N_{Air}^{in} and effect of the air stoichiometry λ_{Air}. Fuel cell fed by dry hydrogen and air at 70% RH. $\lambda_{H_2} = 1.4$, $T = 70\ ^\circ C$ and $P = 1.6$ bar.

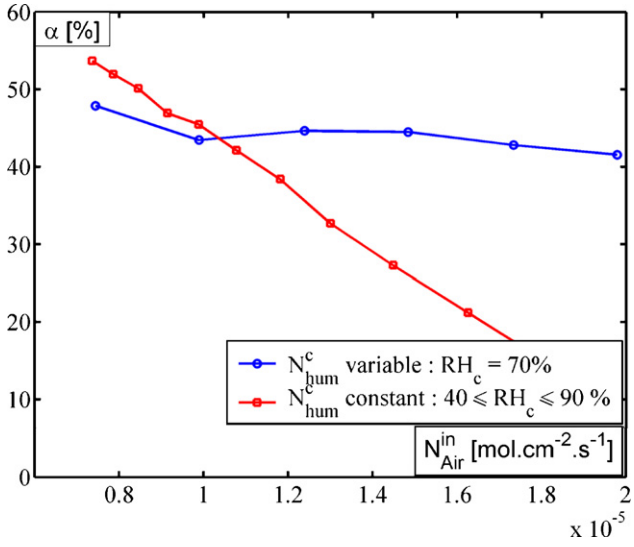

Fig. 8. Variations in α as a function of the air flow rate N_{Air}^{in} and effect of the humidification strategy. Fuel cell fed by dry hydrogen and wet air at constant (RH_c = 70%) or varying RH (90 > RH_c > 40%). $\lambda_{H_2} = 1.4$, T = 70 °C and P = 1.6 bar.

on the current density when the air stoichiometry is set to $\lambda_{Air} = 2$ or $\lambda_{Air} = 2.5$.

As shown in [21], liquid water is present in most of the cases at the outlet of each electrode. An increase in the air flow rate results in a slight decrease of the amount of liquid water at the anode side (from 80% to 77%) and to a significant reduction of the amount of liquid water at the cathode exit (from 32% to 0%), as presented by Santarelli et al. [42] in a PEMFC stack. There is no more liquid water at the cathode outlet when λ_{Air} is above 3.5. However, α does not vary significantly if λ_{Air} increases up to 4, which could mean that the water transport coefficient does not depend on the state of water in the cathode channel, but rather on the state of water at a location closer to membrane, for instance at the electrodes.

In Fig. 7, the air relative humidity is maintained constant (RH_c = 70%), which requires to adapt the water flow rate at the cathode inlet to the air flow rate and to the stoichiometric ratio, according to Eq. (1). A different way to proceed consists in keeping $N_{H_2O}^{Hum}$ at a constant value and to let the relative humidity RH_c vary. In the example presented in Fig. 8 below, $N_{H_2O}^{Hum} = 1.55 \times 10^{-6}$ mol cm^{-2} s^{-1}. The airflow ranges from $N_{Air}^{in} = 7.3 \times 10^{-6}$ mol cm^{-2} s^{-1} to $N_{Air}^{in} = 18.4 \times 10^{-6}$ mol cm^{-2} s^{-1} (corresponding to an air stoichiometric ratio $1.5 < \lambda_{Air} < 3.75$) at constant current density (j = 0.4 A cm^{-2}), so that 90% > RH_c > 40%. The resulting decrease in the air inlet relative humidity entails a decrease in α. Fig. 8 shows that the humidification strategy has a strong effect on water transport. This point is discussed in the next section.

4.2. Water flow rate at the cathode inlet

According to Eq. (1) and keeping constant the other parameters, the humidification water flow rate at the cathode inlet $N_{H_2O}^{Hum}$ can be expressed as a function of the air stoichiometric ratio, relative humidity, temperature, and pressure. The experimental variation ranges corresponding to each of these parameters are listed in Table 3.

Fig. 9 depicts the water transport coefficient α as a function of the water flow rate $N_{H_2O}^{Hum}$ at the cathode inlet in the four

Table 3
Variation ranges of the water flow rate at the cathode inlet $N_{H_2O}^{Hum}$ resulting from variations in λ_{Air}, RH_c, T and P. j = 0.4 A cm^{-2}.

Case	λ_{Air} (-)	RH_c (%)	T (°C)	P (bar)	$N_{H_2O}^{Hum}$ (mol . cm^{-2}. s^{-1})
1 - λ_{Air} variable	1.5 ... 4	70	70	1.6	1.16 ... 3.1 × 10^{-6}
2 - RH_c variable	2	10 ... 90	70	1.6	0.2 ... 2.09 × 10^{-6}
3 - T variable	2	70	50 ... 80	1.6	0.56 ... 2.57 × 10^{-6}
4 - P variable	2	70	70	1 ... 1.6	2.74 ... 1.55 × 10^{-6}

cases described above, the current density being kept constant (j = 0.4 A cm^{-2}). In a general manner, the water transport coefficient varies between 10% and 55%. α appears to be a strong function of the cathode humidification water flow rate only when its variations result from those of the air relative humidity and of the temperature. On the other hand, the air stoichiometry (i.e., the air flow rate) and the pressure do not seem to be meaningful parameters.

4.2.1. Air stoichiometry

As discussed in Section 4.1 and depicted in Figs. 7 and 8, when variations in $N_{H_2O}^{Hum}$ result from those of λ_{Air} (varying between 1.5 and 4), the water transport coefficient decreases of only 5% (from 50% to 45%).

4.2.2. Pressure

Note that since it is dangerous to impose a high pressure difference between both sides of the membrane, the values applied to the air and hydrogen flows are identical. As shown in Fig. 9, when the pressure decreases from 1.6 to 1 bar, the water transport coefficient increases slightly. Moreover, over the whole pressure range, gases issued from the anode and cathode sides remained saturated with vapor. Yan et al. [29] obtained a similar trend by decreasing the pressure from 2 to 1 bar.

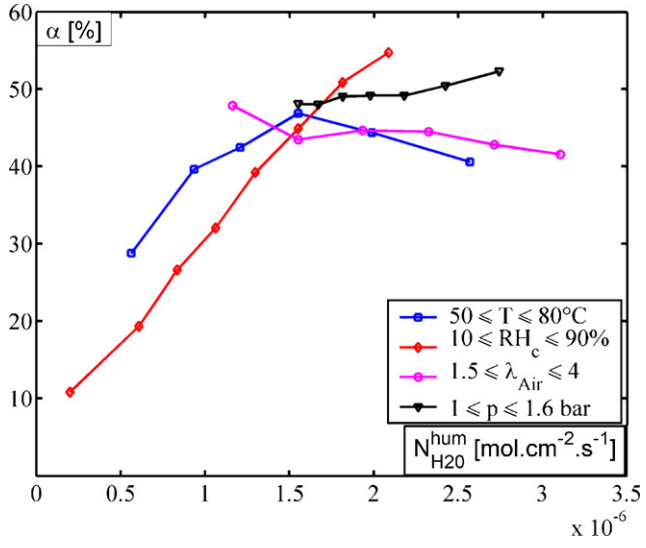

Fig. 9. Water transport coefficient α vs. the cathode inlet water flow rate $N_{H_2O}^{Hum}$. The significance of $N_{H_2O}^{Hum}$ depends on the origin of its variations (Table 3).

4.2.3. Air relative humidity

In Table 3, the air inlet relative humidity RH_c ranges from 10% to 100%, resulting in an increase from 0.2×10^{-6} mol cm^{-2} s^{-1} to 2.09×10^{-6} mol cm^{-2} s^{-1} of the water flow rate at the cathode inlet (Eq. (1)) whereas the other parameters are kept constant. As shown in Fig. 9, the vapor flow rate $N_{H_2O}^{Hum}$ has a strong effect on the amount of water collected at the anode side: the water transport coefficient α increases almost linearly from 10% to 55% with the relative humidity of air.

Water is transported through the membrane mainly by diffusion and electro-osmosis. Since the sensitivity study described in this section was carried out at constant current density, the electro-osmotic flow can be assumed constant (although strictly speaking it may depend also on the membrane water content [9]), which means that only the diffusion flux varies with the air inlet relative humidity. As it rises from 10% to 100% while the hydrogen remains dry, the water gradient through the membrane increases (at least at the cell inlet), as well as the diffusion flux from the cathode to the anode. This trend was already observed by several authors [25,30–33,35].

The ratio of liquid water reaches 40% of the total amount collected at the cathode outlet. On the other hand, when the cathode is fed by almost dry air (RH_c < 10%), the saturation is not reached at the outlet.

4.2.4. Temperature

Fig. 9 shows the dependence of the water transport coefficient on the fuel cell temperature. The inlet temperature of the gases is equal to that of the fuel cell: it varies from 50 to 80 °C, which corresponds to a vapor flow rate at the cathode inlet ranging from 0.56×10^{-6} mol cm^{-2} s^{-1} to 2.57×10^{-6} mol cm^{-2} s^{-1}.

Below 70 °C, the water transport coefficient increases significantly with the temperature. This trend was also reported by Büchi and Srinivasan [22] with a fuel cell fed by dry hydrogen and dry air. The maximal value of α (45%) is observed at T = 70 °C. Above this value, α decreases lightly, from 45% to 40%. Two phenomena can be at the origin of this behaviour:

- The vapor saturation pressure increases with the temperature, as well as the amount of water that can be removed in vapor phase at the both electrodes, as shown in Table 4. Since the airflow at the cathode exit is higher than the residual hydrogen flow at the anode, the water transport coefficient is expected to decrease as the temperature rises, which is observed only above 70 °C.
- The effective water diffusion coefficient in the membrane $D_{H_2O}^{m}$ increases also with the temperature. According to Fuller and Newman [51], it can be expressed as follows:

$$D_{H_2O}^{m}(\lambda, T) = 3.5 \times 10^{-6} \frac{\lambda}{14} \exp\left(-\frac{2436}{T}\right) \quad (8)$$

The water flux through the membrane can be calculated as follows:

$$N_{H_2O}^{Diff} = -D_{H_2O}^{m} \frac{dc_{H_2O}}{dx} \quad (9)$$

Integrating this equation over the membrane thickness and expressing the result as a function of its water content at the cathode, λ_c, and at the anode, λ_a yields:

$$N_{H_2O}^{Diff} = -\frac{3.5 \times 10^{-6}}{14} \exp\left(-\frac{2436}{T}\right) \frac{\rho_{dry}}{EW} \frac{\lambda_c^2 - \lambda_a^2}{2E_m} \quad (10)$$

The values of the water flux calculated for λ_c = 11 and λ_a = 10 and presented in Table 5 show that the amount of water transported by diffusion through the membrane is a strong function of the temperature, which can explain the increase in α below 70 °C. However, these results are only indicative since the membrane water content is probably not homogeneous over the whole surface of the electrodes.

Table 4
Amounts of water needed to saturate the gas flows at the anode and the cathode outlet as functions of the temperature. Fuel cell fed by dry hydrogen and air at 70% RH. λ_{Air} = 2; λ_{H_2} = 1.4 and P = 1.6 bar.

	T (°C)					
	50	60	65	70	75	80
Anode 10^{-6} (mol cm^{-2} s^{-1})	0.066	0.11	0.15	0.19	0.25	0.33
Cathode 10^{-6} (mol cm^{-2} s^{-1})	0.18	0.32	0.43	0.59	0.81	1.14

Table 5
Water diffusion flux through the membrane as a function of the temperature according to Eq. (10). λ_a = 10; λ_c = 11 and $E_m = 40 \times 10^{-6}$ m.

	T (°C)					
	50	60	65	70	75	80
$N_{H_2O}^{Diff}$ 10^{-6} (mol cm^{-2} s^{-1})	6.4	8	8.9	9.9	11	12.1

4.2.5. Conclusion on the significance of the water flow rate at the cathode inlet

From the results presented on Fig. 9, it can be also concluded that, at a current density of 0.4 A cm^{-2}, the temperature and the air inlet relative humidity are the two main parameters affecting significantly the water transport coefficient α.

4.3. Air relative humidity

In the previous section, the sensitivity study on air relative humidity was carried out at constant current density and it is necessary to check whether this conclusion applies to variable load.

According to Eq. (1), and keeping the stoichiometric ratio constant, each value of the vapor flow rate at the cathode inlet defines a relation between the current density j and the air relative humidity RH_c. For example, $N_{H_2O}^{Hum} = 1.32 \times 10^{-6}$ mol cm^{-2} s^{-1} corresponds to {j = 0.5 A cm^{-2} with RH_c = 50%} and to {j = 0.25 A cm^{-2} with RH_c = 90%}. Fig. 10 presents curves of the water transfer coefficient vs. the water flow rate at the cathode inlet obtained by varying the current density and by keeping the air inlet relative humidity constant (RH_c = 50%, 70% and 90%). The values measured at con-

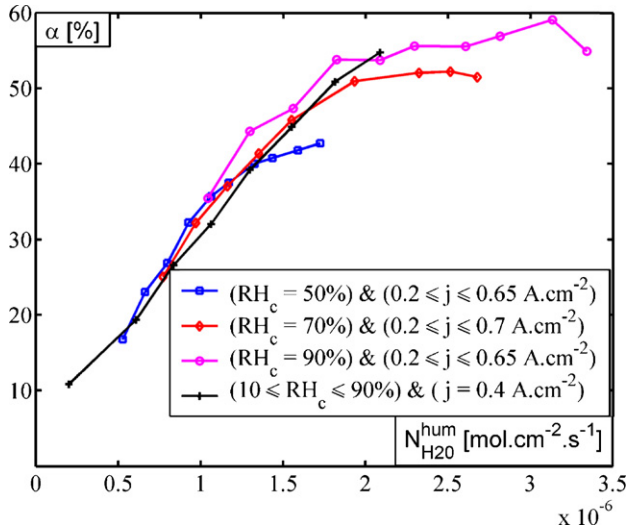

Fig. 10. α as a function of the vapor flow rate at cathode inlet $N_{H_2O}^{Hum}$ and effect of the air inlet relative humidity RH_c. Fuel cell fed by dry hydrogen, λ_{Air} = 2; T = 70 °C and P = 1.6 bar.

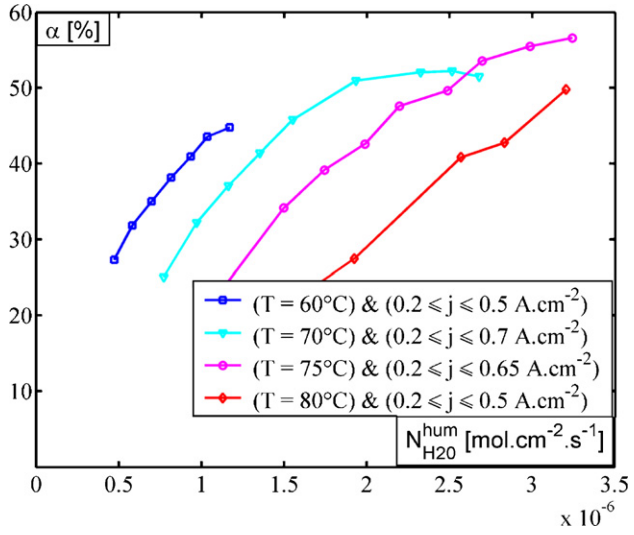

Fig. 11. Variations in α as a function of the vapor flow rate at the cathode inlet $N_{H_2O}^{Hum}$ and effect of the temperature. Fuel cell fed by dry hydrogen, $\lambda_{H_2} = 1.4$; $RH_c = 70\%$; $\lambda_{Air} = 2$ and $P = 1.6$ bar.

stant current density ($j = 0.4\,A\,cm^{-2}$) by increasing the air relative humidity presented in Fig. 9 are included for comparison.

As observed in Fig. 10, the water transport coefficient increases with the current density whatever the air inlet relative humidity. Moreover, it can be noticed that the curves obtained for the three values of the air relative humidity are very close to each other and are similar to the results obtained at constant density: this means that the parameter that governs the flux of water from anode to cathode is the cathode humidification water flow rate, rather than the current density or the air inlet relative humidity.

As j rises, the air inlet relative humidity decreases if $N_{H_2O}^{Hum}$ is kept constant, but the amount of water necessary to saturate the gases at the anode and at the cathode increases, as well as the production of water at the cathode. There is a competition between the water diffusion through the membrane and the water removal through the air channels, which does not seem to depend on other operating parameter than the vapor flow rate at the cathode inlet $N_{H_2O}^{Hum}$.

4.4. Cell temperature

As shown in Section 4.2, at constant current density, the temperature is one of the parameters influencing the flux of water from anode to cathode, although less significant than the air relative humidity. Fig. 11 presents curves of the water transfer coefficient vs. the water flow rate at the cathode inlet obtained by varying the current density and by keeping the temperature constant ($T = 60\,^{\circ}C$, $70\,^{\circ}C$, $75\,^{\circ}C$ and $80\,^{\circ}C$): for each temperature, the water transport coefficient increases with the current density but the four curves are clearly different.

Keeping the vapor flow rate at the cathode inlet constant, the water transport coefficient α decreases as the temperature increases: $N_{H_2O}^{Hum} = 1.55 \times 10^{-6}\,mol\,cm^{-2}\,s^{-1}$ corresponds for instance to $\alpha = 45\%$ at $70\,^{\circ}C$ and to $\alpha = 20\%$ at $80\,^{\circ}C$. These two results correspond also to different current densities ($j = 0.4\,A\,cm^{-2}$ at $70\,^{\circ}C$ and $j = 0.25\,A\,cm^{-2}$ at $80\,^{\circ}C$) but as discussed in Section 4.3, for given water flow rate at the cathode inlet $N_{H_2O}^{Hum}$, α does not depend on the current density. The effects of the temperature on the water transfer coefficient observed in Fig. 11 are identical to those discussed in Section 4.2.

5. Conclusion

The operation of a PEM 5-cells pilot stack fed by dry hydrogen was investigated from the point of view of water transfer, its electrical performances having already been discussed in a previous paper [21]. The water transport coefficient was measured over a wide range of operating conditions.

Contrary to the electrical performances, the water transport coefficient is insensitive to aging, which allows the comparison between data measured at different period of the fuel cell lifetime. The results reveal that 20–60% of water produced at the cathode flows through the membrane to the anode. Surprisingly, this percentage increases with the current density and then stabilizes at the highest values ($0.5 \leq j \leq 0.7\,A\,cm^{-2}$). This indicates that the diffusion through the membrane is the dominant process for the water transport and distribution within the cell, while the effects of electro-osmosis are not observed directly. The whole of the results are in good agreement with values and trends reported in the literature.

The water transport coefficient depends on the current density, flow rate and humidification of the gases. Increasing the hydrogen stoichiometry ratio entails an increase in the water transport coefficient. However, in the tested range of current density and hydrogen stoichiometry, the parameter governing water transfer within the cell seems to be the hydrogen flow rate rather than the current density. The results are more difficult to interpret at the cathode. At constant values of temperature and current density, the relative humidity of air appears to be the main parameter governing the water transport coefficient. On the other hand, if the temperature only is kept constant, the water transport coefficient depends on the vapor flow rate at the cathode inlet. As far as the temperature is concerned, increasing its value improves the water diffusion coefficient through the membrane (which tends to increase the water transport coefficient) but it enhances also the vapor removal capacity of the airflow (through an increase in the vapor saturation pressure). The first effect dominates below $70\,^{\circ}C$, then the water transport coefficient decreases.

In most of the cases, liquid water is present at the cathode outlet and also at the anode outlet. Visualizing liquid water in-situ during fuel cell operation and understanding fully the water transport mechanisms are the two important issues for improving the performances and the reliability of PEMFC.

References

[1] W. Winkler, VDI Berichte 2036 (2008) 15–33.
[2] T.V. Nguyen, Electrochem. Soc. Trans. 3 (1) (2006) 1171–1180.
[3] P. Sauriol, G.-S. Kim, H.T. Bi, J. Stumper, J. St-Pierre, AIChE Annual Meeting, 2005.
[4] T.A. Zawodzinski, C. Derouin, S. Radzinski, R.J. Sherman, V.T. Smith, T.E. Springer, S. Gottesfeld, J. Electrochem. Soc. 140 (4) (1993) 1041–1047.
[5] G. Maranzana, O. Lottin, T. Colinart, S. Chupin, S. Didierjean, J. Power Sources 180 (2) (2008) 748–754.
[6] H. Li, Y. Tang, Z. Wang, Z. Shi, S. Wu, D. Song, J. Zhang, K. Fatih, J. Zhang, H. Wang, Z. Liu, R. Abouatallah, A. Mazza, J. Power Sources 178 (1) (2008) 103–117.
[7] U. Pasaogullari, in: S. Kakaç, A. Pramuanjaroenkij, L. Vasiliev (Eds.), Mini-Micro Fuel Cells, Springer, Dochdrecht, 2008, pp. 171–188.
[8] T.E. Springer, T.A. Zawodzinski, S. Gottesfeld, J. Electrochem. Soc. 138 (8) (1991) 2334–2342.
[9] D.M. Bernardi, M.W. Verbrugge, AIChE J. 37 (8) (1991) 1151–1163.
[10] T. Colinart, S. Didierjean, O. Lottin, G. Maranzana, C. Moyne, J. Electrochem. Soc. 155 (3) (2008) B244–B257.
[11] J.H. Nam, M. Kaviany, Int. J. Heat Mass Transfer 46 (24) (2003) 4595–4611.
[12] J. Ramousse, J. Deseure, O. Lottin, S. Didierjean, D. Maillet, J. Power Sources 145 (2) (2005) 416–427.
[13] O. Lottin, B. Antoine, T. Colinart, S. Didierjean, G. Maranzana, C. Moyne, J. Ramousse, Int. J. Thermal Sci. 48 (1) (2009) 133–145.
[14] N. Djilali, P.C. Sui, Int. J. Comp. Fluid Dynamics 22 (1–2) (2008) 115–133.
[15] M.A. Hickner, N.P. Siegel, K.S. Chen, D.S. Hussey, D.L. Jacobson, M. Arif, J. Electrochem. Soc. 155 (4) (2008) B427–B434.
[16] M.A. Hickner, N.P. Siegel, K.S. Chen, D.S. Hussey, D.L. Jacobson, M. Arif, J. Electrochem. Soc. 155 (3) (2008) B294–B302.

[17] K. Yoshizawa, K. Ikezoe, Y. Tasaki, D. Kramer, E.H. Lehmann, G.G. Scherer, J. Electrochem. Soc. 155 (3) (2008) B223–B227.
[18] P. Boillat, D. Kramer, B.C. Seyfang, G. Frei, E. Lehmann, G.G. Scherer, A. Wokaun, Y. Ichikawa, Y. Tasaki, K. Shinohara, Electrochem. Com. 10 (4) (2008) 546–550.
[19] S. Tsushima, K. Teranishi, S. Hirai, Electrochem. Solid-state Lett. 7 (9) (2004) A269–A272.
[20] J. Bedet, G. Maranzana, S. Leclerc, O. Lottin, C. Moyne, D. Stemmelen, P. Mutzenhardt, D. Canet, Int. J. Hydrogen Energy 33 (12) (2008) 3146–3149.
[21] C. Bonnet, S. Didierjean, N. Guillet, S. Besse, T. Colinart, P. Carré, J. Power Sources 182 (2) (2008) 441–448.
[22] F.N. Büchi, S. Srinivasan, J. Electrochem. Soc. 144 (8) (1997) 2767–2772.
[23] D. Picot, R. Metkemeijer, J.J. Bezian, L. Rouveyre, J. Power Sources 75 (2) (1998) 251–260.
[24] K.H. Choi, D.H. Peck, C.S. Kim, D.R. Shin, T.H. Lee, J. Power Sources 86 (1–2) (2000) 197–201.
[25] G.J.M. Janssen, M.L.J. Overvelde, J. Power Sources 101 (1) (2001) 117–125.
[26] M. Ciureanu, M. Badita, J. New Mater. Electrochem. Syst. 6 (2003) 163–168.
[27] T. Mennola, M. Noponen, T. Kallio, M. Mikkola, T. Hottinen, J. Appl. Electrochem. 34 (1) (2004) 31–36.
[28] Y. Cai, J. Hu, H. Ma, B. Yi, H. Zhang, Electrochem. Acta 51 (28) (2006) 6361–6366.
[29] Q. Yan, H. Togiani, J. Wu, J. Power Sources 158 (14) (2006) 316–325.
[30] T. Murahashi, M. Naiki, E. Nishiyama, J. Power Sources 162 (2) (2006) 1130–1136.
[31] S.U. Jeong, A.E. Cho, H.J. Kim, T.H. Lim, I.H. Oh, S.H. Kim, J. Power Sources 159 (2) (2006) 1089–1094.
[32] H.K. Atiyeh, K. Karan, B. Peppley, A. Phoenix, E. Hlliop, J. Pharoah, J. Power Sources 170 (1) (2007) 111–121.
[33] K. Karan, A. Phoenix, E. Hlliop, J. Pharoah, B. Peppley, Electrochem. Solid-State Lett. 10 (2) (2007) B34–B38.
[34] G.Q. Lu, F.Q. Liu, C.Y. Wang, J. Power Sources 164 (1) (2007) 134–140.
[35] F.Q. Liu, G.Q. Lu, C.Y. Wang, J. Membr. Sci. 287 (1) (2007) 126–140.
[36] D.R. Sena, E.A. Ticianelli, V.A. Paganin, E.R. Gonzalez, J. Electroanal. Chem. 477 (2) (1999) 164–170.
[37] T. Abe, H. Shima, K. Watanabe, Y. Ito, J. Electrochem. Soc. 151 (1) (2004) A101–A105.
[38] N. Rajalakshmi, P. Sridhar, K.S. Dhathathreyan, J. Power Sources 109 (2) (2002) 452–457.
[39] N. Rajalakshmi, T.T. Jayanth, R. Thangamuthu, G. Sasikumar, P. Sridhar, K.S. Dhathathreyan, Int. J. Hydrogen Energy 29 (10) (2004) 1009–1014.
[40] M.V. Williams, H.R. Kunz, J.M. Fenton, J. Power Sources 135 (1–2) (2004) 122–134.
[41] M.G. Santarelli, M.F. Torchio, Energy Convers. Manage. 48 (1) (2007) 40–51.
[42] M.G. Stantarelli, M.F. Torchio, M. Cali, V. Giaretto, Int. J. Hydrogen Energy 32 (6) (2007) 710–716.
[43] S. Ge, C.Y. Wang, J. Electrochem. Soc. 154 (10) (2007) B998–B1005.
[44] H. Nakajima, T. Konomi, T. Kitahara, J. Power Sources 171 (2) (2007) 457–463.
[45] http://www.helion-hydrogen.com/.
[46] F. Harel, X. François, D. Candusso, M.-C. Péra, D. Hissel, J.-M. Kauffmann, Fuel Cells 7 (2) (2007) 142–152.
[47] E. Guilminot, A. Corcella, M. Chatenet, F. Maillard, F. Charlot, G. Berthomé, C. Iojoiu, J.Y. Sanchez, E. Rossinot, E. Claude, J. Electrochem. Soc. 154 (11) (2007) B1106–B1114.
[48] C. Iojoiu, E. Guilminot, F. Maillard, M. Chatenet, J.Y. Sanchez, E. Claude, E. Rossinot, J. Electrochem. Soc. 154 (11) (2007) B1115–B1120.
[49] C. Lee, W. Merida, J. Power Sources 164 (1) (2007) 141–153.
[50] Y. Wang, D.O. Northwood, Adv. Mater. Res. 41–42 (2008) 469–475.
[51] T.F. Fuller, J. Newman, J. Electrochem. Soc. 140 (5) (1993) 1218–1225.